

Supplement of Atmos. Chem. Phys., 15, 2327–2340, 2015  
<http://www.atmos-chem-phys.net/15/2327/2015/>  
doi:10.5194/acp-15-2327-2015-supplement  
© Author(s) 2015. CC Attribution 3.0 License.



*Supplement of*

## **Oxidant production from source-oriented particulate matter – Part 1: Oxidative potential using the dithiothreitol (DTT) assay**

**J. G. Charrier et al.**

*Correspondence to:* C. Anastasio ([canastasio@ucdavis.edu](mailto:canastasio@ucdavis.edu))

## S1. Mass dependence of the mass-normalized DTT response

The mass-normalized DTT rate is commonly used to compare the oxidative potential of different particle types. A previously unappreciated complication with this technique is that, for samples with appreciable DTT loss due to Cu and/or Mn, the value of the mass-normalized DTT rate depends on the PM mass concentration used in the DTT assay. This is because the DTT responses from Cu and Mn are non-linear (Charrier and Anastasio, 2012). We are currently working to develop and validate a method to deal with this artifact to create a true “mass normalized” DTT response that can be compared between different studies. While we will publish the results from this work in a forthcoming study, below we describe the current version of our normalization procedure.

Because the Cu and Mn DTT responses are non-linear, a true comparison of DTT rates requires either that all samples are studied using the same particle mass concentration in the DTT extract (which is difficult to accomplish) or that the results be normalized to a standard mass concentration. In either case, we recommend as the standard mass concentration  $10 \mu\text{g PM mL}^{-1}$  of solution, which is near the middle of the range of values we typically use.

To calculate the DTT response at  $10 \mu\text{g PM mL}^{-1}$  we first calculate the DTT response from Mn and Cu in the DTT extract based on their measured concentrations. The remaining DTT response (i.e., the component not explained by Cu and Mn) is labeled as “unknown”. We then calculate the DTT responses expected from Cu and Mn in a  $10 \mu\text{g PM mL}^{-1}$  extract of the sample (assuming that the concentrations of Cu and Mn vary linearly with the PM mass) using the non-linear concentration-response curves from Charrier and Anastasio (2012). We assume the DTT responses of the unknown redox-active species vary linearly with PM mass to determine the DTT response expected from the unknown species at  $10 \mu\text{g PM mL}^{-1}$ ; we previously showed that the concentration-response curves for redox-active species other than Cu and Mn (e.g., for Fe and quinones) are linear in Charrier and Anastasio (2012). We then sum the calculated responses from Cu, Mn and unknown species to get the mass-normalized DTT response at  $10 \mu\text{g PM mL}^{-1}$ .

Figure S1 shows a graphical example of normalization for one sample from the current work (Winter CV4 sub-micron fine, i.e., W4SMF) in units of  $\mu\text{M DTT/min}$  and  $\text{pmols DTT/min}/\mu\text{g PM}$  in panels a and b, respectively. The black “X” in the figure represents the measured DTT response in this sample, which was determined using a mass concentration of  $10.5 \mu\text{g mL}^{-1}$  and had corresponding Cu and Mn concentrations of 0.062 and 0.015  $\mu\text{M}$ . From these Cu and Mn concentrations we calculate their expected DTT responses as a function of sample mass concentration: these are represented by the purple and green lines, respectively. The expected response from the unknown redox-active species is shown by the orange line, while the total sample response (sum of Cu, Mn, and unknowns) expected as a function of mass is shown by the blue line. From this line we can determine the expected DTT response at any sample mass concentration; the red star shows the calculated DTT response at a PM concentration of  $10 \mu\text{g PM mL}^{-1}$ . For this sample the measured mass-normalized DTT rate is 37.4  $\text{pmols/min}/\mu\text{g PM}$ , while the calculated rate at  $10 \mu\text{g PM mL}^{-1}$  is 38.3  $\text{pmols/min}/\mu\text{g PM}$ .

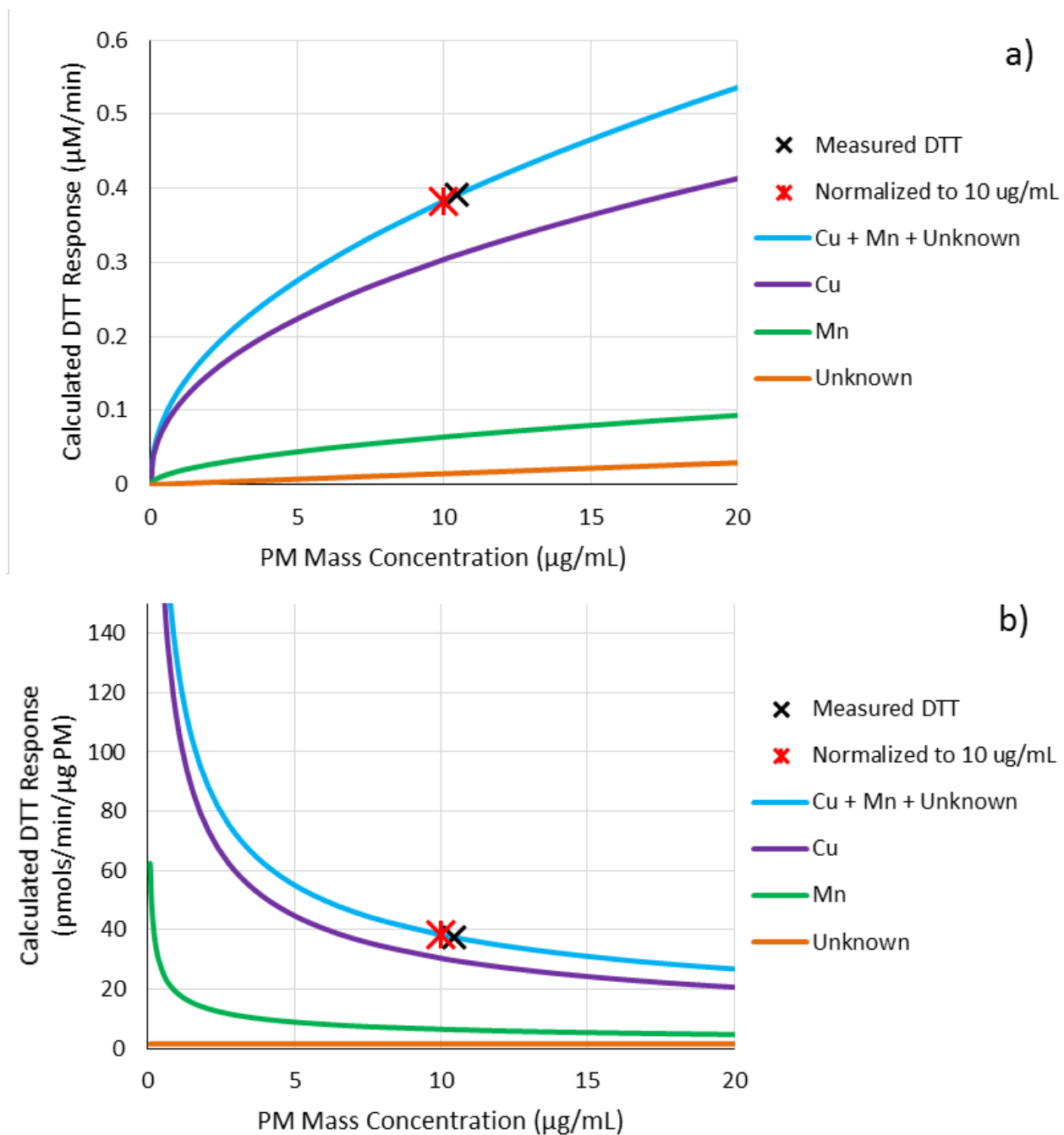


Figure S1. An example of DTT normalization to a PM mass concentration of  $10 \mu\text{g mL}^{-1}$  for a) units of  $\mu\text{M DTT / min}$  and b) units of  $\text{pmols}/\text{min}/\mu\text{g PM}$ . The black "X" shows the measured DTT response and the red star shows the DTT response normalized to  $10 \mu\text{g PM mL}^{-1}$ . Cu (purple), Mn (green) and unknown (orange) DTT responses were calculated as a function of PM mass based on measured soluble metals and concentration response curves from (Charrier and Anastasio, 2012), and assuming the unknown response is linear. The upper blue line shows the total calculated DTT response from the sum of Cu, Mn and unknown species.

We applied this current normalization procedure to all of the samples. As illustrated for sample S2SMF above, the mass-normalized DTT responses are, overall, not substantially changed when

calculated to  $10 \mu\text{g PM mL}^{-1}$ . This is because most samples were measured using a similar mass concentration: the average ( $\pm 1 \sigma$ ) mass concentration for our samples was  $9.7 \pm 3.0 \mu\text{g mL}^{-1}$ . Figure S2 shows the close agreement between the measured and calculated mass-normalized DTT responses for all samples. Figure S3a shows the comparison of measured and normalized DTT responses for each sample. Though the difference in measured and normalized DTT rates is not generally large, the normalized DTT rate has much larger error bars because it also includes the propagated errors from the soluble metals measurements: the average RSD for the measured values is 23%, while the corresponding value for the normalized samples is 46%. As shown in Figure S3b, out of the 38 samples, there is only one where the difference between normalized and measured is more than one standard deviation from zero.

Based on these small differences between normalized and measured DTT rates, and the large increase in error associated with normalizing for these extracts, we have not normalized the DTT response for these PM samples in the main text. We are working on a manuscript that discusses this normalization procedure and its application to a subsequent set of samples that do show a large bias based on PM mass concentration. As we discuss in the forthcoming manuscript, some PM samples will have to be normalized to correctly interpret the results, especially samples that have a high contribution from Cu and Mn and that were determined with a mass concentration very different than  $10 \mu\text{g PM mL}^{-1}$ . The non-linear responses from Cu and Mn complicate the interpretations of DTT data in past studies, where the contributions of these transition metals were not assessed.

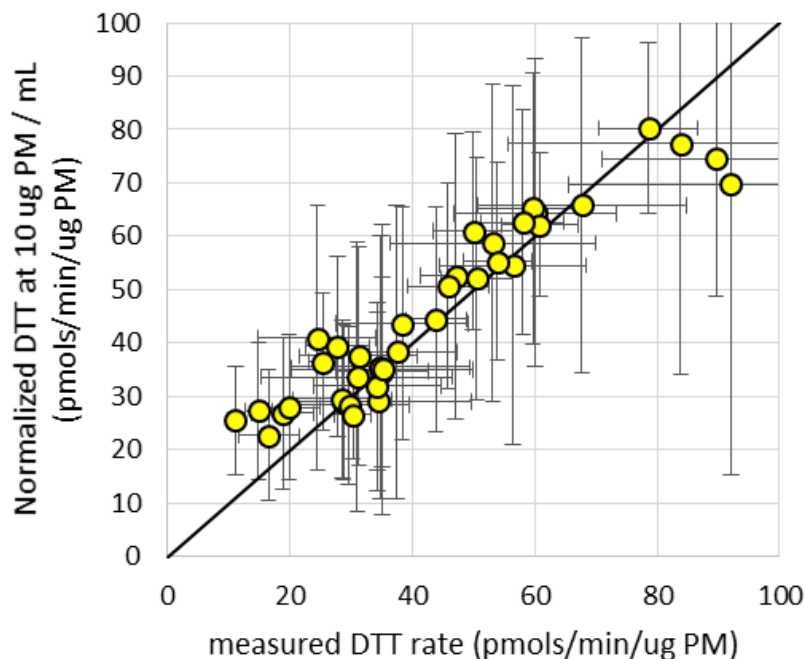


Figure S2. Measured DTT rate versus the rate when normalized to  $10 \mu\text{g PM mL}^{-1}$ . The black line represents the 1:1 line. Error bars represent  $\pm 1 \sigma$  of propagated error from all sources (PM mass added to the vial, DTT rate, and soluble metals measurements).

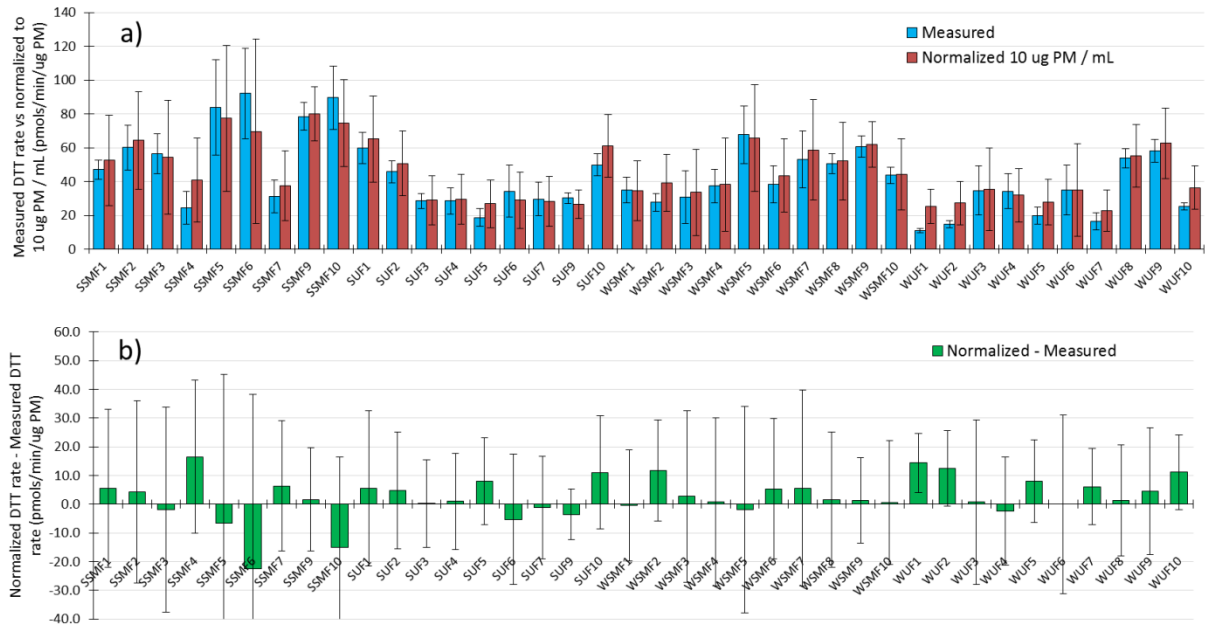


Figure S3. Measured versus normalized DTT rate a) for each sample pair, and b) absolute difference. Error bars of normalized DTT rate include propagated error of soluble metals data.

## S2. Soluble metals measurements in DTT solution compared to in surrogate lung fluid

Soluble metals were measured in a surrogate lung fluid (SLF) containing 114 mM NaCl, 2.2 mM  $\text{KH}_2\text{PO}_4$ , 7.8 mM  $\text{Na}_2\text{HPO}_4$  and anti-oxidants (200  $\mu\text{M}$  ascorbic acid, 300  $\mu\text{M}$  citric acid, 100  $\mu\text{M}$  glutathione and 100  $\mu\text{M}$  uric acid), pH of 7.4. Portions of filters were extracted from 1.5 to 24 hours at room temperature on a shake table. DTT assay conditions are somewhat different: the extraction fluid contains 22 mM  $\text{KH}_2\text{PO}_4$ , 78 mM  $\text{Na}_2\text{HPO}_4$  and 100  $\mu\text{M}$  DTT, pH 7.4, and is extracted for 20 minutes at 37  $^\circ\text{C}$ . Both the SLF and DTT extraction solutions were treated with Chelex 100 resin to remove transition metals prior to adding the antioxidants or DTT. The differences in ligands, extraction time and temperature for the two assays could affect soluble metals measurements. To test this, we measured soluble metals under the DTT assay conditions for 12 of the 38 samples (6 summer and 6 winter, 7 SMF and 5 UF). The resulting soluble metal concentrations were very similar for the SLF and DTT extractions, with the exception of (Fig. S4). Fe was sometimes higher in the SLF than the DTT assay, possibly because of the presence of citrate in the SLF, which effectively solubilizes Fe (Aust et al., 2002). Given the similarity in the metals data for the two assays, we use the SLF measurements since these were made for every sample as part of our companion study (Richards-Henderson et al., 2015). The SLF results might sometimes overestimate Fe in the DTT extracts, but this is a minor issue since Fe is nearly always unimportant in the DTT assay (Charrier and Anastasio, 2012).

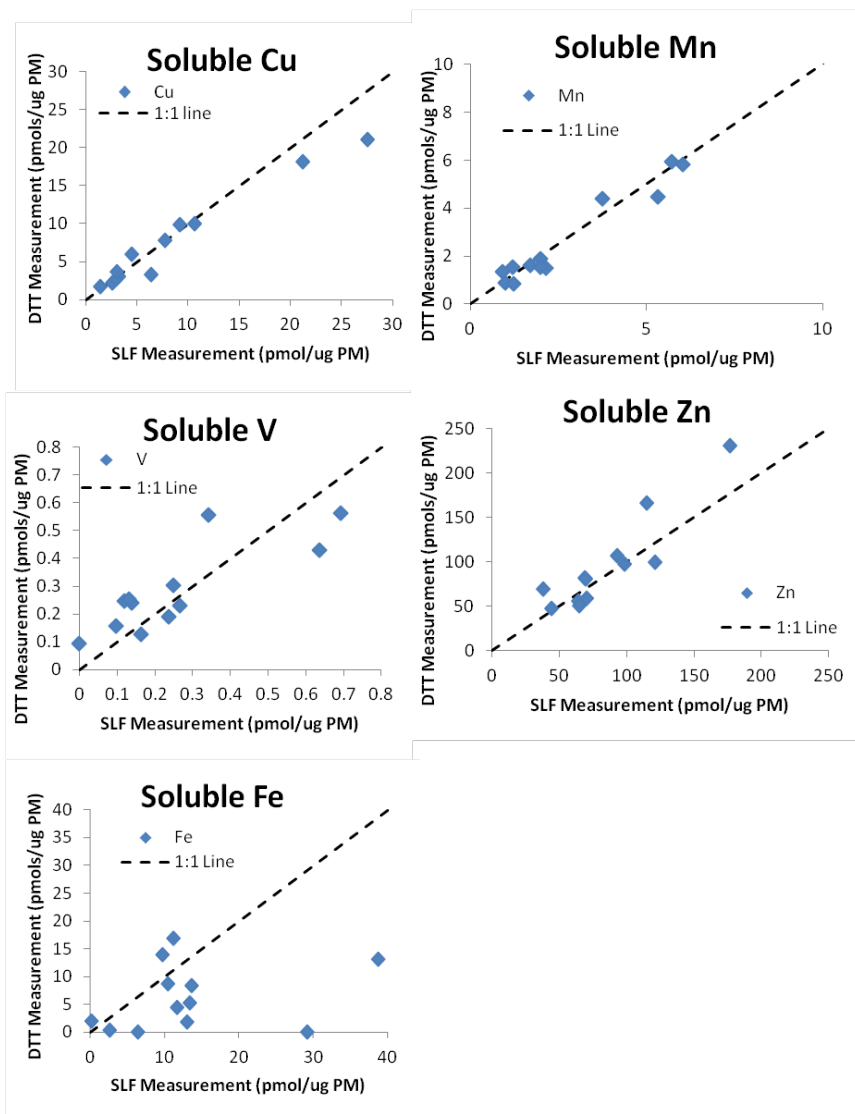


Figure S4. Comparison of soluble metals measurements in DTT solution versus SLF solution.

### S3. Total and soluble metals

To measure total metals, approximately 167  $\mu\text{g}$  of extracted PM from each source was digested using 1 M nitric acid via sonication and diluted to 6 mL for sample analysis. All samples were analyzed in triplicate for a standard set of 26 elements. A description of soluble metals analysis steps is in Section 2.5 of the main text.

Both total and soluble metals were analyzed by the Interdisciplinary Center for Plasma Mass Spectrometry at the University of California at Davis (ICPMS.UCDavis.edu) using an Agilent 7500CE ICP-MS (Agilent Technologies, Palo Alto, CA). The prepared samples were introduced using a MicroMist Nebulizer (Glass Expansion) into a temperature controlled spray chamber with He as the collision cell gas. Instrument standards were diluted from Certiprep ME2A standard (SPEX CertiPrep) to 0.25ppb, 0.5ppb, 1ppb, 10ppb, 100ppb, 200ppb and 500ppb respectively in 3% Trace Element  $\text{HNO}_3$  in ultrapure water. A NIST 1643E Standard was analyzed initially and QC standard consisting of ME2A at 100ppb were analyzed every 12th sample as quality controls. An internal standard consisting of Sc, Y, and Bi Certiprep standards (SPEX CertiPrep) were diluted to 100ppb in 3%  $\text{HNO}_3$  and introduced by peripump. Soluble metals results are in the main text Fig. 1, while total metals results are in Fig. S5 below.

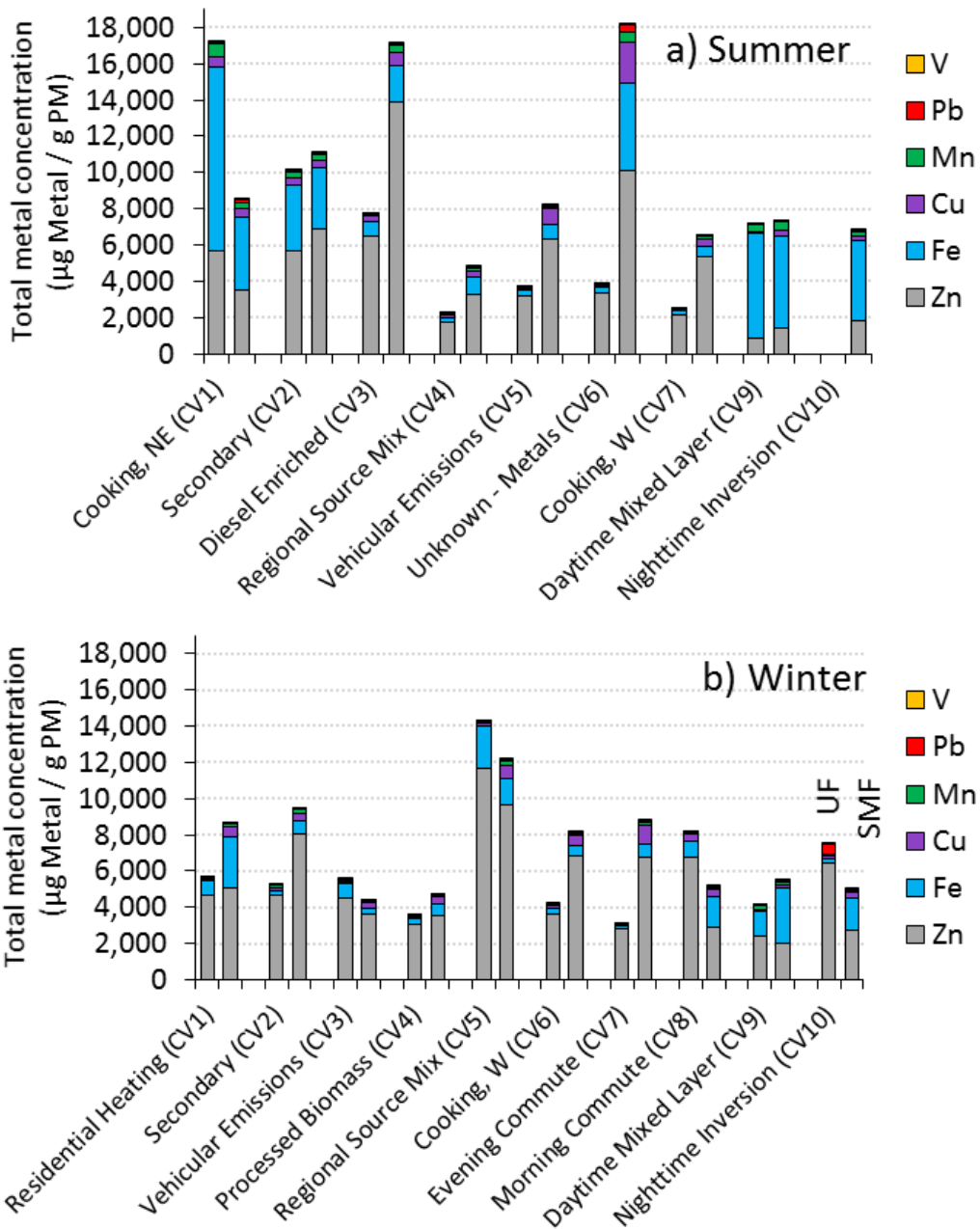


Figure S5. Total metals concentration in each sample. For each CV, the first bar is the UF size fraction and the second bar is the SMF size fraction. Zn concentrations are divided by 10. In panel (a) there is no data for the CV 10 UF sample.

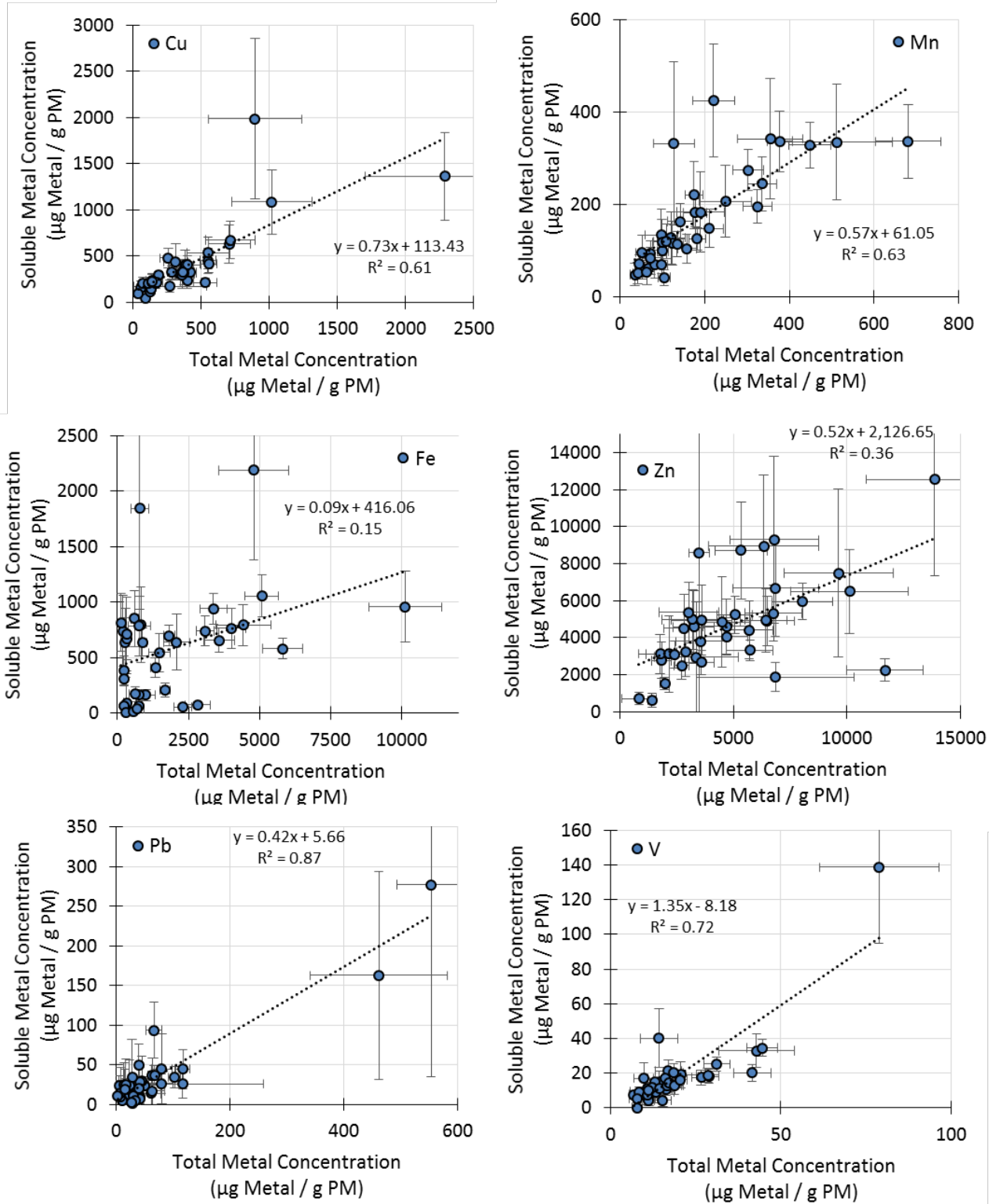


Figure S6. Correlations between total and soluble metals data.

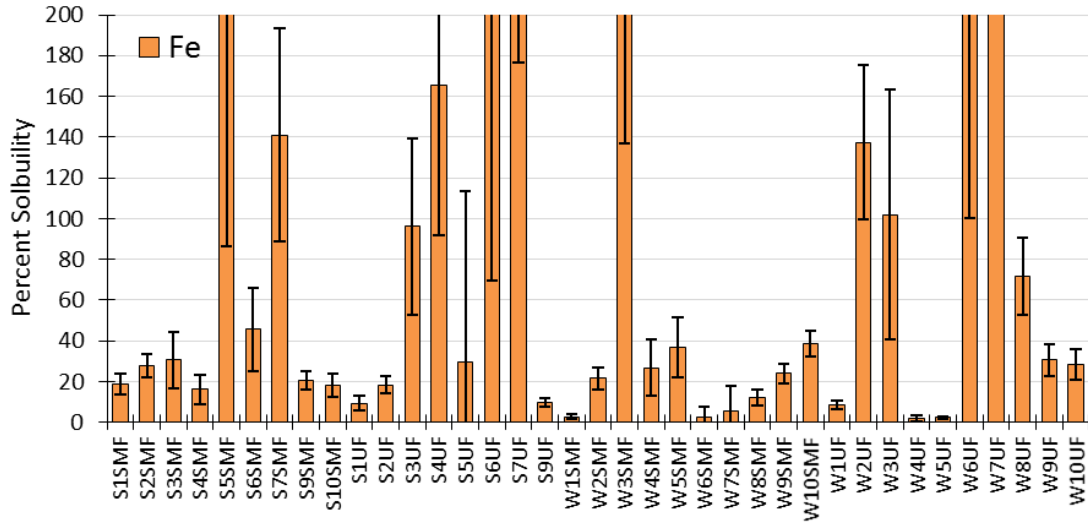
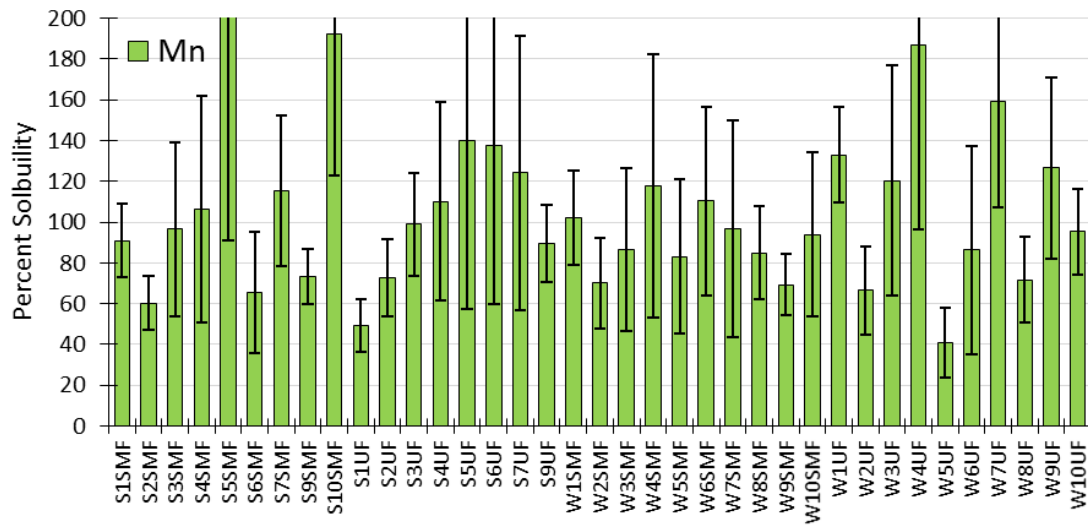
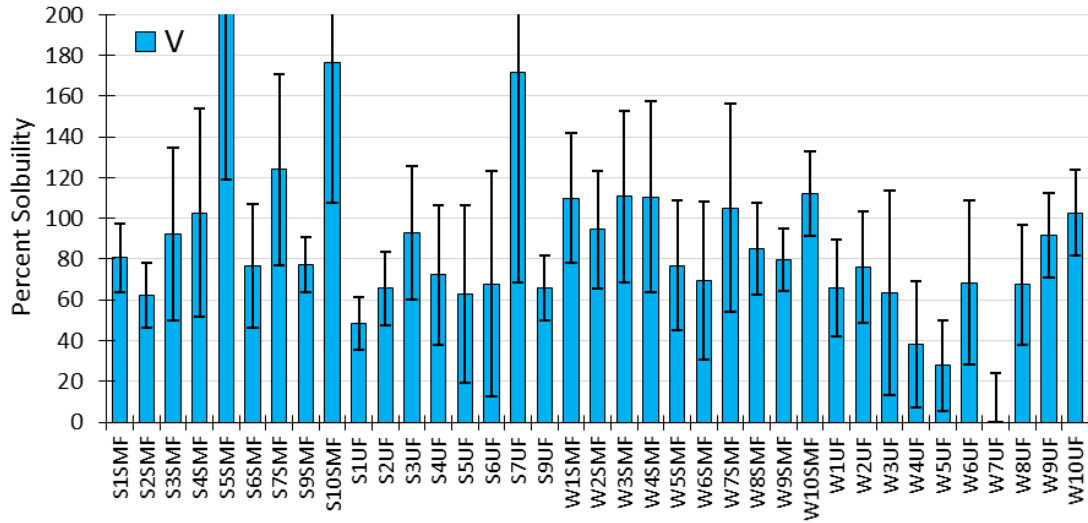
Table S1. Range of atmospheric concentrations of total and soluble metals for each season and size fraction

Metal	Total Metals Median and Range of Concentration (ng/m <sup>3</sup> )			
	Summer 2008		Winter 2009	
	UF	SMF	UF	SMF
Zn	12 (1.9-20)	29 (8.8-128)	19 (4.7-60)	31 (4.7-79)
Ba	4.4 (1.3-11)	4.0 (0.89-7.8)	8.9 (1.1-34)	1.6 (0.30-4.9)
Fe	1.8 (0.40-31)	31 (3.1-44)	2.6 (0.30-12)	6.1 (2.7-24)
Cu	0.44 (0.15-1.7)	4.3 (1.9-21)	0.68 (0.092-1.2)	3.5 (0.42-6.3)
Mn	0.32 (0.084-2.1)	2.3 (0.72-4.7)	0.42 (0.10-0.63)	0.72 (0.30-1.9)
Ni	0.13 (0.091-0.44)	0.80 (0.50-2.5)	0.27 (0.033-1.0)	0.65 (0.21-2.0)
Pb	0.079 (0.013-0.31)	0.56 (0.20-4.2)	0.092 (0.005-1.1)	0.25 (0.12-0.51)
V	0.044 (0.02-0.13)	0.24 (0.087-0.61)	0.051 (0.018-0.11)	0.07 (0.032-0.16)
Cr	0.056 (0.018-0.26)	0.66 (0.24-10)	0.13 (0-0.29)	0.25 (0.14-0.82)
Cd	0.01 (0.005-0.022)	0.05 (0.035-0.17)	0.03 (0.004-0.098)	0.044 (0.013-0.39)
Co	0.009 (0.004-0.041)	0.055 (0.027-0.16)	0.017 (0.002-0.025)	0.032 (0.014-0.12)
Metal	Soluble Metals Median and Range of Concentration (ng/m <sup>3</sup> )			
	Summer 2008		Winter 2009	
	UF	SMF	UF	SMF
Zn	10 (1.6-18)	44 (3.8-116)	15 (6.0-44)	35 (3.6-77)
Ba	3.7 (0.70-5.3)	2.8 (0.36-8.2)	4.6 (0.63-14)	0.78 (0.19-3.3)
Fe	2.0 (0.34-2.9)	6.2 (1.5-20)	1.0 (0.053-5.9)	1.5 (0.16-5.6)
Cu	0.65 (0.11-1.3)	3.7 (1.6-15)	0.79 (0.21-2.0)	3.0 (0.51-6.2)
Mn	0.47 (0.10-1.0)	2.3 (0.83-3.3)	0.42 (0.12-0.79)	0.74 (0.28-1.6)
Ni	0.16 (0.057-0.87)	0.61 (0.16-1.5)	0.28 (0.086-2.6)	0.12 (0-5.0)
Pb	0.058 (0.016-0.10)	0.31 (0.05-1.)	0.14 (0.024-0.53)	0.077 (0.01-0.17)
V	0.039 (0.025-0.16)	0.21 (0.11-1.1)	0.028 (0-0.074)	0.066 (0.036-0.18)
Cr	0.084 (0.034-0.73)	0.34 (0.098-0.56)	0.12 (0.029-0.40)	0.074 (0-0.35)
Cd	0.005 (0-0.50)	0.068 (0-1.2)	0.052 (0-5.6)	0.028 (0-0.32)
Co	0.007 (0.004-0.065)	0.046 (0.022-0.085)	0.021 (0.002-0.34)	0.017 (0.004-0.098)

Note: Co, Cr, Cd and Ni were generally below their detection limits.

#### S4. Percent solubility

We calculated the percent of each metal that was soluble in SLF for each CV and size range as the ratio between the SLF-soluble concentration and the total metal (acid-extract) concentration. Figure S6 shows the percent solubility for the 6 metals that are well measured: V, Mn, Cu, Fe, Zn, Pb. Four metals were generally below detection: Co, Cr, Cd. Total metals data for summer ultrafine “Nighttime Inversion (CV10)” is missing, so percent solubility for that CV cannot be calculated. V, Mn, Cu and Zn all exhibited nearly 100% solubility. Pb is less soluble, with a median solubility of 48% and Fe was generally the least soluble metal measured, with a median solubility of 27%.



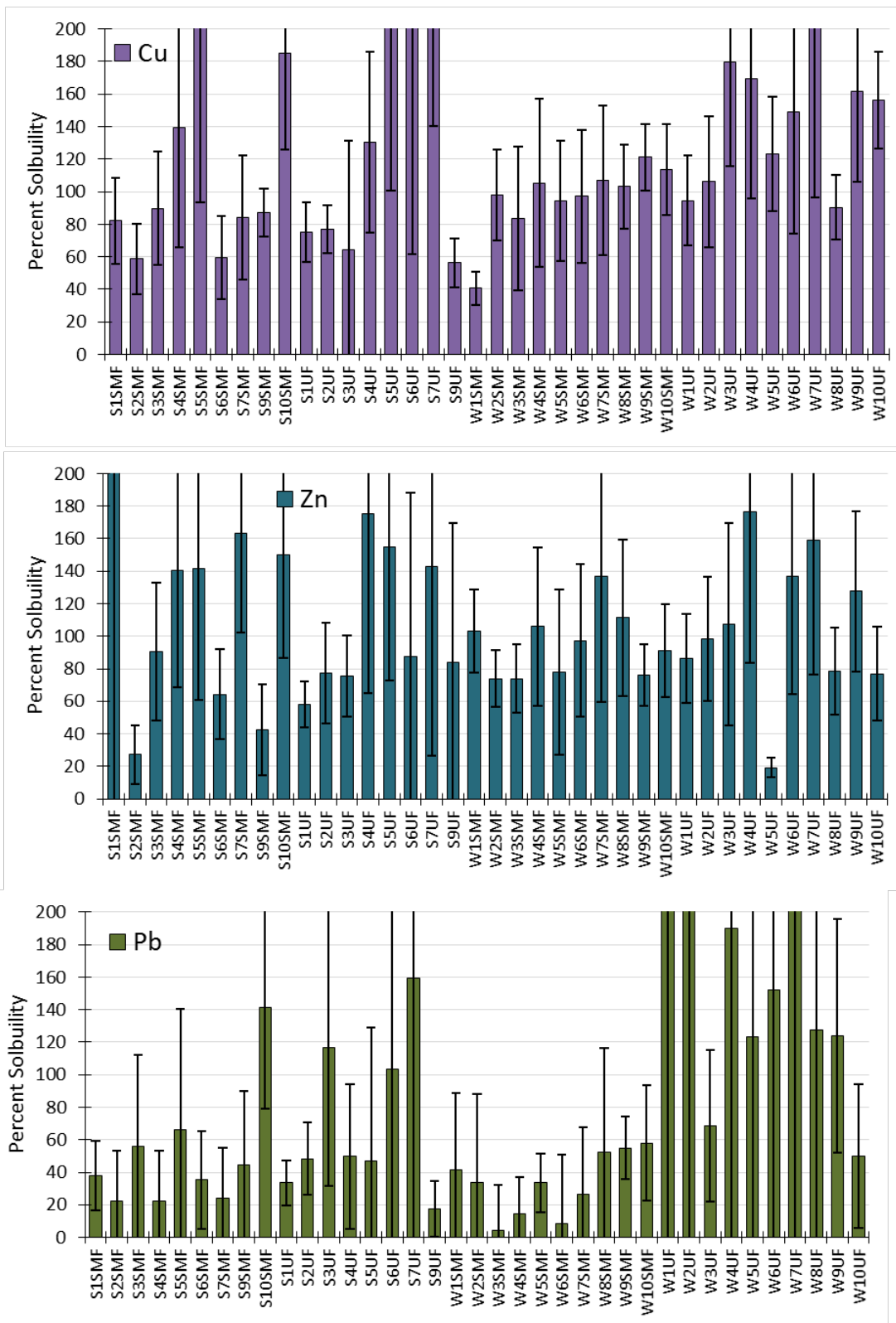


Figure S7. Percent solubility for each metals and CV. Error bars are the propagated errors of soluble and total metals data accounting for both blank corrections and error in the mass data.

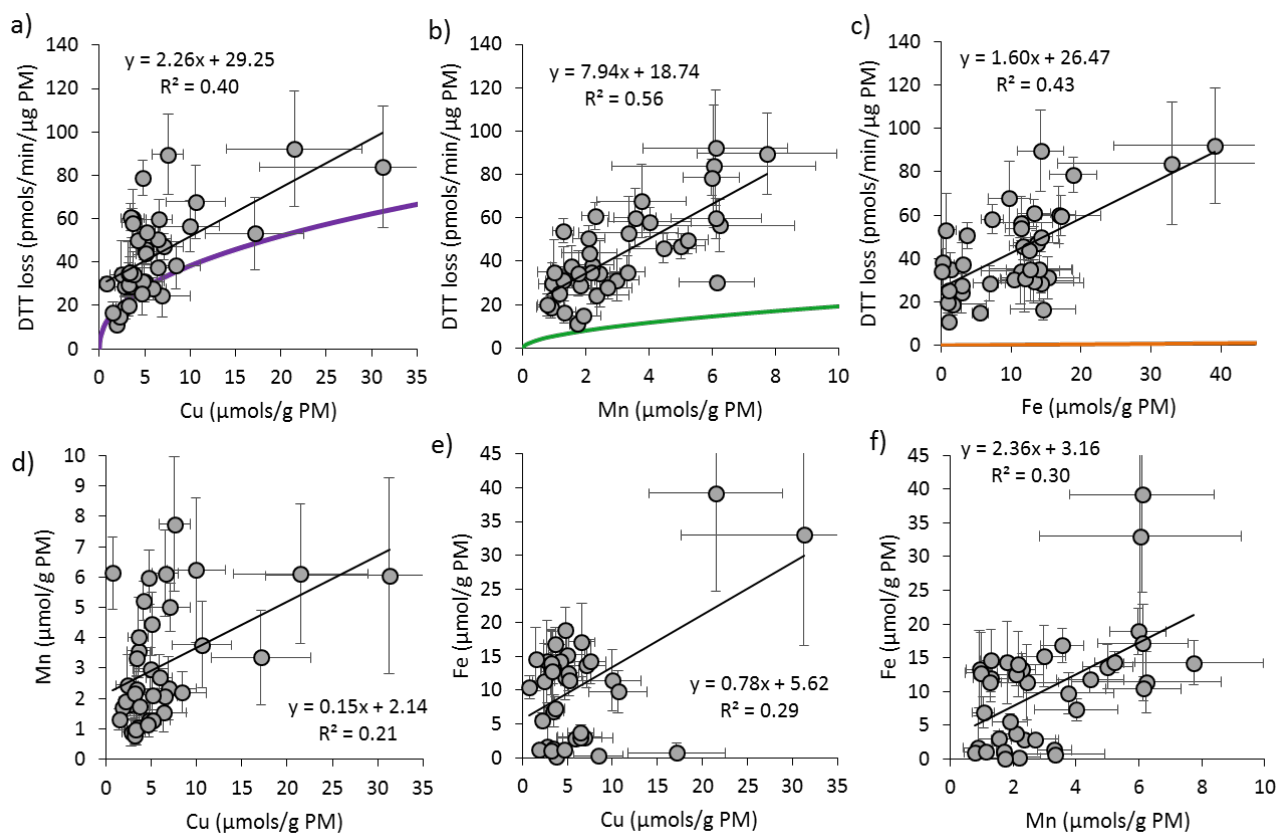


Figure S8. Correlations of DTT loss with soluble Cu, Mn, and Fe (a – c) and correlations between these soluble metal concentrations (d – f). The lines in a – c represent the calculated DTT response as a function of metal concentration for 30  $\mu\text{g}$  of PM based on the concentration-response curves in Charrier and Anastasio (2012) (purple in (a) for pure Cu, green in (b) for pure Mn and orange in (c) for pure Fe).

Table S2. PM masses used for DTT analysis (sample volume is 3.0 mL).

Experiment	ChemVol	UF		SMF	
		Mass ( $\mu\text{g}$ )	Error	Mass ( $\mu\text{g}$ )	Error
<b>Summer 2008 Samples</b>	1	38.2	3.8	38.2	3.8
	2	38.2	3.8	38.2	3.8
	3	29.4	3.7	28.0	5.6
	4	31.4	7.8	36.1	9.0
	5	24.7	6.2	18.7	6.2
	6	18.0	6.0	17.6	4.4
	7	17.6	4.4	31.4	6.3
	9	9	0.3	32.3	3.2
	10	56.8	N/A	18.2	3.6
	<b>Winter 2009 Samples</b>	1	37.3	3.9	29.4
2		29.4	3.9	29.4	4.2
3		31.4	6.7	29.4	4.2
4		24.7	6.7	31.4	7.8
5		31.4	3.9	28	7.0
6		30	7.5	28	7.0
7		29.4	4.5	20.0	5.0
8		32.3	3.3	32.3	3.2
9		39.0	4.4	32.3	3.2
10		8	0.6	31.0	3.1
<b>Field Blanks</b>		2.0	--	2.0	--

#### S5. Estimating the contribution of PQN to DTT response

To test if PQN is likely important in our samples we assume ambient particulate PQN was present at the median measured concentration previously reported ( $0.3 \text{ ng/m}^3$ ) (Charrier and Anastasio, 2012). Using the mass concentration of each sample (Table 1 in the main text) and the mass of PM added to each vial (Table S2), we calculated the expected concentration of PQN in each solution. We then used the PQN concentration-response equation from Charrier and Anastasio (2012) to calculate the DTT response from PQN in each DTT extract and calculated what percent of the DTT response this would contribute to each sample. Results are discussed in the main text.

#### S6. Apportionment of volume-normalized oxidative potential to individual sources.

We categorized the sources we observed and those in the modeling of Hu et al. (2014) into four categories: Cooking, Mobile, Heating, Biomass/Wood Smoke. Any sources that do not fit these categories are labeled "Other". The sources included in each category are listed in Supplemental Tables S3 and S4. We calculated the average ambient mass concentration for each category over our two-week sampling periods using the 7-year average source contributions from 2000 – 2006 provided in Hu et al.

(2014). We multiplied the mass concentration of each category by the weighted average of the mass-normalized oxidative potential (Fig. 2) for the associated category to get the volume-normalized oxidative potential of each category. We then summed the volume-normalized oxidative potential of each category (Fig. 4c and 4d). There is a remaining volume-normalized oxidative potential measured from the PM which is not accounted for by the four source categories. We attribute this to “Unknown” sources, which includes the “Other” category, sources that were not identified in the emissions inventory, and secondary PM mass, which is not accounted for in the primary modeling data of Hu et al. A large percent of PM mass is identified in “Other”, which consists of constrained and unconstrained PM sources (Fig. S9).

Our approach makes several assumptions. First, our measurements are for  $PM_{1.0-0.17}$  and  $PM_{0.17}$ , while corresponding model results are for  $PM_{2.5}$  and  $PM_{0.1}$ , respectively. Secondly, our samples were collected in 2008 and 2009 while model sources are from 2000 – 2006. And finally, model sources only account for primary PM mass, so contribution from secondary PM mass is automatically grouped into “Unknown”. Though these assumptions are not ideal, the data from Hu et al. (2014) are the most complete estimates of PM sources in Fresno currently available, especially in regards to the ultrafine size fraction.

Table S3. ARB emissions inventory PM sources from (Hu et al., 2014) with their associated category.

<b>Source</b>	<b>Category</b>
Agricultural pruning waste burning	Biomass/Wood Smoke
Agricultural crop waste burning	Biomass/Wood Smoke
Residential wood stoves	Biomass/Wood Smoke
Residential wood fireplaces	Biomass/Wood Smoke
Non-agricultural waste burning	Biomass/Wood Smoke
Commercial deep fat frying	Cooking
Commercial cooking unspecified	Cooking
Commercial Charbroiling	Cooking
Industrial residual oil combustion	Heating
Residential natural gas water heating	Heating
Residential natural gas space heating	Heating
Offroad trans refrigeration diesel	Mobile
offroad industrial diesel equipment	Mobile
Ag. Irrigation diesel engines	Mobile
Light commercial gasoline equipment	Mobile
Light commercial diesel equipment	Mobile
Lawn and garden gasoline 2-st	Mobile
Onroad diesel exhaust	Mobile
lawn and garden diesel equipment	Mobile
Construction and mining diesel	Mobile
Industrial gasoline equipment 4-st	Mobile
Lawn and garden gasoline 4-st	Mobile
Onroad non-cat. gasoline hot exhaust	Mobile
Trains hauling locomotives	Mobile
Stationary IC diesel engines	Mobile
Agricultural diesel equipment	Mobile
Recreational gasoline boat (unspec) 2-st	Mobile
Onroad cat. gasoline hot exhaust	Mobile
Cat. gasoline buses	Mobile
Onroad cat. gasoline cold exhaust	Mobile
Onroad diesel idle	Mobile
Non-cat. gasoline cold exhaust	Mobile
Onroad diesel buses	Mobile
Construction and mining gasoline	Mobile
Paved road dust freeways	Mobile
Paved road dust local streets	Mobile
Paved road dust major streets	Mobile
Commercial natural gas combustion	Other
Commercial LPG combustion	Other
Ag. land windblown dust	Other
Commercial bldg construction&demolition	Other
Farming tilling dust	Other
Industrial bldg construction&demolition	Other
Institutional bldg construction&demolition	Other
Non-constrained PM2.5 sources	Other
Unpaved road dust farm roads	Other
Oil drill diesel equipment	Other
Other constrained PM0.1 sources	Other
Other constrained PM2.5 sources	Other
Residential bldg construction&demolition	Other
Stationary IC diesel engines	Other
Structural fires	Other
Non-constrained PM0.1 sources	Other

Table S4. Sources identified during our sampling with associated categories.

<b>CV</b>	<b>Source</b>	<b>Category</b>
<b>Summer</b>		
1	Cooking - NE	Cooking
7	Cooking - W	Cooking
3	Diesel enriched	Mobile
5	Vehicular emissions	Mobile
2	Secondary	Other
4	Regional source mix	Other
6	Unknown - metals	Other
10	Nighttime Inversion	Other
9	Daytime mixed layer	Other
<b>Winter</b>		
4	Processed biomass	Biomass
6	Cooking - W	Cooking
1	Residential heating	Heating
3	Vehicular emissions	Mobile
8	Morning commute	Mobile
2	Secondary	Other
5	Regional source mix	Other
10	Nighttime inversion	Other
9	Daytime mixed layer	Other
7	Evening commute	Other

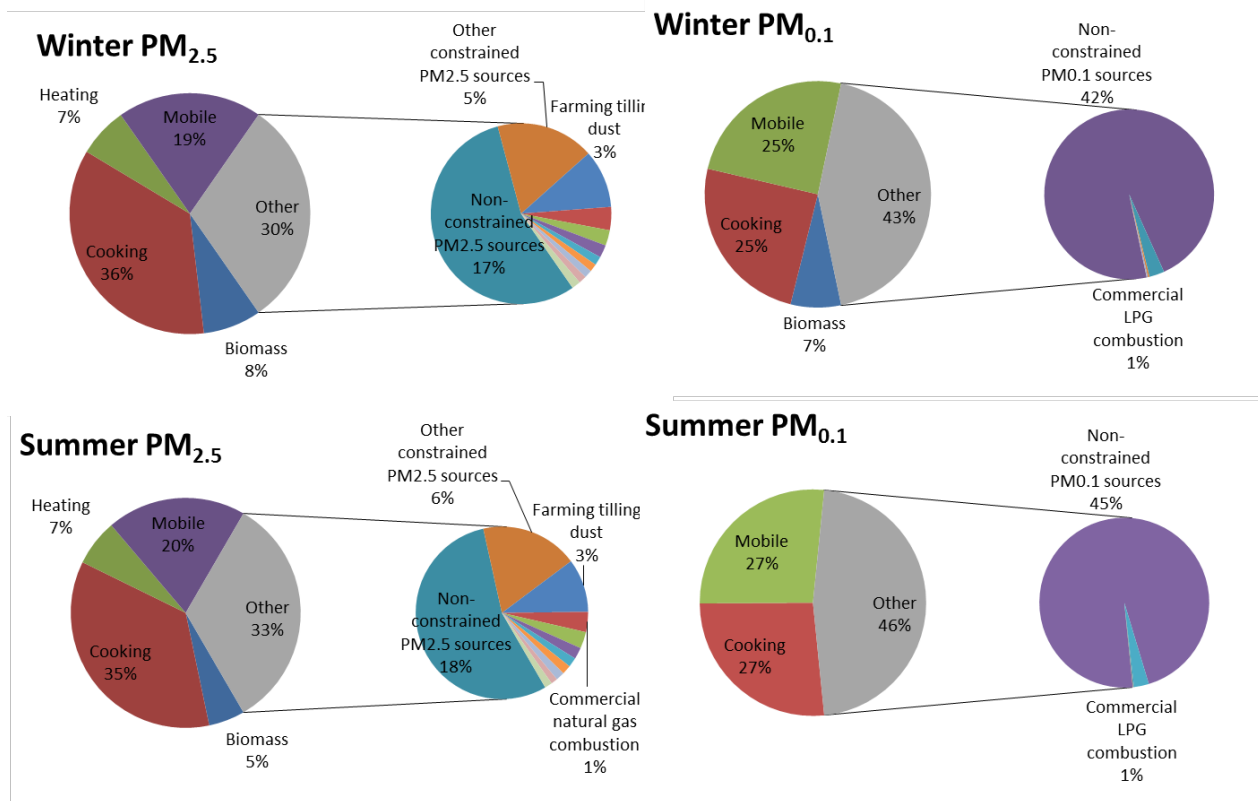


Figure S9. Contribution of source categories to total primary PM mass in Fresno, CA as identified by modeling for the time period that match ambient samples (Hu et al., 2014). To match previous nomenclature, “winter” is actually 3/1/2009 to 4/6/2009 and “summer” is actually 9/11/2008 to 10/21/2008 is designated “summer” (see main text methods discussion). A detailed summary of sources contributing to the “Other” category is shown in each expansion pie charts.

## References

- Aust, A. E., Ball, J. C., Hu, A. A., Lighty, J. S., Smith, K. R., Straccia, A. M., Veranth, J. M., and Young, W. C.: Particle characteristics responsible for effects on human lung epithelial cells, Research Report/Health Effects Institute, 1-65; discussion 67-76, 2002.
- Charrier, J. G., and Anastasio, C.: On dithiothreitol (DTT) as a measure of oxidative potential for ambient particles: evidence for the importance of soluble transition metals., *Atmos. Chem. Phys.*, **12**, 9321-9333, 2012.
- Hu, J., Hongliang, Z., Chen, S., Ying, Q., Wiedinmyer, C., Vandenberghe, F., and Kleeman, M.: Identifying PM<sub>2.5</sub> and PM<sub>0.1</sub> sources for epidemiological studies in California, *Env. Sci. Technol.*, **48**, 4980-4990, 2014.
- Richards-Henderson, N. K., Charrier, J. G., Bein, K. J., Bau, D., Wexler, A. S., and Anastasio, C.: Oxidant production from source-oriented particulate matter – Part 2: Hydrogen peroxide and hydroxyl radical, *Atmos. Chem. Phys.*, In Preparation, 2015.